AGU PUBLICATIONS

Water Resources Research

RESEARCH ARTICLE
10.1002/2014WR016484

Johnson SB as general functional form for raindrop size distribution

Katia Cugerone[1] and Carlo De Michele[1]

[1]Department of Civil and Environmental Engineering, Politecnico di Milano, Piazza Leonardo da Vinci 32, 20133 Milano, Italy

Key Points:
- For the first time, the Johnson SB distribution is proposed for the statistical description of DSDs
- Large disdrometric data sets are analyzed to compare the fit of Johnson SB, Gamma and Lognormal distributions
- Skewness-kurtosis plane, AIC-BIC indices and K-S goodness-of-fit test have been used

Supporting Information:
- Supporting Information S1

Correspondence to:
C. De Michele,
carlo.demichele@polimi.it

Citation:
Cugerone, K., and C. De Michele (2015), Johnson SB as general functional form for raindrop size distribution, *Water Resour. Res.*, *51*, 6276–6289, doi:10.1002/2014WR016484.

Received 30 SEP 2014
Accepted 6 JUL 2015
Accepted article online 14 JUL 2015
Published online 13 AUG 2015

Abstract Drop size distribution represents the statistical synthesis of rainfall dynamics at particle size scale. Gamma and Lognormal distributions have been widely used in the literature to approximate the drop diameter variability, contrarily to the natural upper boundary of the variable, with almost always site-specific studies and without the support of statistical goodness-of-fit tests. In this work, we present an extensive statistical investigation of raindrop size distribution based on eight data sets, well distributed on the Earth's surface, which have been analyzed by using skewness-kurtosis plane, AIC and BIC indices and Kolmogorov-Smirnov test. Here for the first time, the Johnson SB is proposed as general functional form to describe the drop diameter variability specifically at 1 min time scale. Additional analyses demonstrate that the model is well suitable even for larger time intervals ($\geq$1 min).

1. Introduction

Rainfall remains one of the poorly quantified phenomena of the hydrological cycle, despite its fundamental role [*De Michele and Ignaccolo*, 2013]. No universal law describing the rainfall behavior is available in the literature. This is probably due to the continuous description of rainfall, which is a discrete phenomenon, made by drops [*Ignaccolo and De Michele*, 2011]. Raindrops represent the water exchange, under liquid form, between atmosphere and earth surface, and the number of drops and their size have impacts in a wide range of hydrologic, meteorologic, and ecologic phenomena [*Norman et al*., 1995; *Pruppacher and Klett*, 2010; *Strangeways*, 2011].

From the statistical point of view, the rainfall variability at particle size scale is described by the *drop size distribution* (DSD). According to the specific problem of interest, the term DSD indicates the concentration of raindrops per unit volume and diameter, $\mathcal{N}(D)$, or the probability density function of drop diameter at the ground, $p(D)$. These two quantities are linked together and it is possible to pass from one to the other; for additional details see *Uijlenhoet and Pomeroy* [2001] and *Ignaccolo and De Michele* [2013]. It is noteworthy that rainfall is a nonhomogeneous phenomenon [*Jameson and Kostinski*, 2001; *Ignaccolo et al*., 2009], thus, regardless of the form used, the "statistical rule" with which the drops occur is not invariant under time translation. For this, DSD must be referred to small time intervals (DSD observed in 1 min, or less, the so called *instant* DSD), where the phenomenon can be considered homogeneous [*Joss and Gori*, 1978]. DSD is used in many applications, among others, to measure the multiwavelength rain attenuation for terrestrial and satellite systems, to evaluate the below cloud scavenging coefficient of the aerosol by precipitation and to make estimates of rainfall rate through radars, [*Uijlenhoet and Sempere Torres*, 2006]. In particular, DSD is used to evaluate the parameters of the $Z-R$ relationship between reflectivity (Z) and rainfall rate (R). It is well known that variations in the form of DSD are one of the main causes of variability of $Z-R$ parameters [*Jaffrain et al*., 2011; *Rosenfeld and Ulbrich*, 2003; *Tokay et al*., 2001].

For many years, DSD has been represented parametrically by the negative Exponential law, proposed by Marshall and Palmer [*Marshall and Palmer*, 1948; *Laws and Parsons*, 1943]. Nowadays, thanks to advanced instrumentations, disdrometers, which allow to measure the rainfall drop by drop, and collect millions of information per year, it has become clear that the negative Exponential law is a limiting form, resulting from the long-term average in time and space [*Waldvogel*, 1974; *Kostinski and Jameson*, 1999]. In addition, according to many observations, the Exponential law usually underestimates the number of large drops and overestimates the small ones [*Fujiwara*, 1965; *Cataneo and Stout*, 1968]. Other distributions have been adopted [*Williams and Gage*, 2009], including Lognormal [*Feingold and Levin*, 1986; *Rosenfeld and Ulbrich*, 2003;

Owolawi, 2011], Weibull [*Jiang et al*., 1997; *Sekine et al*., 2007; *Ishii et al*., 2011] and, above all, Gamma, with or without truncations [*Ulbrich*, 1983; *Willis*, 1984; *Ulbrich*, 1985; *Ulbrich and Atlas*, 1998; *Illingworth and Blackman*, 2002; *Vivekanandan et al*., 2004; *Brawn and Upton*, 2008; *Kumar et al*., 2011]. This last has been widely used thanks to the parsimonious parameterization and the simple analytic calculation of statistical moments and bulk variables, which are important motivations for practical application. Frequently, the choice of a particular distribution is justified by the fact that it is able to reproduce bulk variables, like the rainfall rate [*Smith et al*., 2009]. However, this criterion could not be considered statistically adequate [*Ignaccolo and De Michele*, 2013]. In the wake of the insights of *Sekhon and Srivastava* [1971], different investigations have been made in order to find a unique mathematical model able to capture the great time and space variability of DSD. These attempts include renormalization and rescaling procedures of different types [see *Sempere Torres et al*., 1994; *Testud et al*., 2001; *Lee et al*., 2004; *Ignaccolo et al*., 2009, among others].

Nevertheless, from the analysis of the literature, some issues emerge:

1. Generally, the used distributions are not upper bounded, in contrast with the lower and upper boundaries of drop diameter, which ranges in a bounded interval. The lower bound corresponds to the smallest diameter of drops having a falling velocity larger than the upward wind speed in the air; minimum sizes occur in case of drizzle (diameter about 0.1 mm) produced by low layer clouds. The maximum diameter of raindrops is about 6–8 mm, different sources provide different values. In any case, the presence of the upper bound is certain: sizes larger than that do not normally occur because the raindrop particles simply break up or collide with other neighboring particles [*Villermaux and Bossa*, 2009].
2. With some exceptions, like *Bringi et al*. [2003] or *Ulbrich and Atlas* [2007], the studies available in the literature are often site-specific, i.e., analyzing the data of a single site. We propose an extensive analysis based on eight data sets, covering several seasons and coming from four different climatic regimes, in order to consider as many precipitation forms and patterns as possible.
3. Lastly, the choice of the probability distribution of drop diameter is actually not supported by statistical tests, as it should be. This is probably due to the large sample size (N) of data, $N \gg 100$, which makes restrictive the application of goodness-of-fit tests.

Dealing with these issues, in the next, we will try to answer to the following question. Is there a general parametric probability distribution, which provides a statistically significant fit to 1 min samples of drop diameter, and respects the natural limits of this variable? Clearly the positive answer to this question must require, as proof, a large set of data, well distributed in space.

2. Probability Model for Drop Size

Here we first propose the *Johnson SB* distribution as a general functional form to describe the variability of the DSD. This is part of the Johnson's system of distributions, made known by Johnson [*Johnson*, 1949], as a flexible model, able to cover a wide variety of distribution shapes. This system is composed by three families, SB (System Bounded), SU (System Unbounded), and SL (System Lognormal), so that any data set with finite moments can be fitted by one of them. The probability density function of a Johnson SB variate X is:

$$p(x)=\frac{\delta}{\sqrt{2\pi}}\cdot\frac{\lambda}{(x-\xi)(\lambda+\xi-x)}\cdot\exp\left\{-\frac{1}{2}\left[\gamma+\delta\ \ln\left(\frac{x-\xi}{\lambda+\xi-x}\right)\right]^2\right\} \tag{1}$$

with $x\in[\xi,\xi+\lambda]$, $-\infty<\xi<\infty$, $\lambda>0$, $-\infty<\gamma<\infty$, and $\delta>0$. ξ and λ are, respectively, the location and scale parameters, ξ and $(\xi+\lambda)$ can be considered proportional to the minimum and maximum value of the variable. γ and δ affect the shape of the distribution. In particular, increasing in absolute value γ increases the skewness, increasing δ increases the kurtosis. Details are available in Appendix A.

We take in consideration the Johnson SB mainly for three reasons. (1) The bounded domain of the variable, which is well suitable for the drop diameter. (2) The existence and the finiteness of all statistical moments, due to the bounded support of the distribution [*Spanos*, 1999]. (3) The great variety of distribution forms, thanks to the two parameters (δ and γ) controlling the shape [*Kotz and Van Dorp*, 2004]. It is able to reproduce various forms: for example, when $\delta\to 0$, regardless of the value of γ, the probability density function becomes bimodal.

Thanks to its flexibility, the Johnson SB distribution has found applications in many fields like meteorology, in particular in the distribution of cloudiness [*Johnson*, 1949] and in the description of the early time stage

Table 1. List of the Sites Where Disdrometer Data Are Collected, With Köppen-Geiger Index in Brackets, Code, Latitude, Longitude, and Altitude

Site	Code	Latitude (°)	Longitude (°)	Altitude (m)
Bukit Koto Tabang, Indonesia (AM)	BKT	0.12S	100.19E	864
Darwin, Australia (AM)	DRW	12.45S	130.83E	12
Estation Obispo, Mexico (BSH)	ETO	24.28N	107.20W	27
Kashima, Japan (CFA)	KSH	35.95S	140.65E	45
Kwajalein Atoll, Marshall Islands (AF)	MIK	8.71N	167.73W	1
Macugnaga, Italy (DFB)	MAC	45.58N	7.57E	1300
Milano, Italy (CFA)	MLN	45.28N	9.23E	123
Torino, Italy (CFA)	TRN	45.03N	7.65E	239

of evolution of drops due to coagulation phenomenon [*Tang and Lin*, 2013]; hydrology, in the distribution of rain rate [*Kottegoda*, 1987] and in the description of the modified relative humidity [*Wakazuki*, 2013], and ecology in the size distribution of trees [*Rennolls and Wang*, 2005]. For these reasons, in this work, Johnson SB distribution will be tested as alternative to Gamma and Lognormal, being the most used distributions to fit the drop diameter data. For all the three distributions, the Maximum Likelihood method has been used to estimate the parameters (see Appendix B for details).

3. Data Processing

We consider eight data sets consisting of 1 min DSD data, sampled using Joss-Waldvogel and Thies disdrometers at different locations on the Earth's surface. Table 1 provides the description of the data sets including name of the site, Köppen-Geiger climatic classification (code between brackets), a three-letter code used to report the name of the measurement site in brevity, latitude, longitude, and altitude. The Köppen-Geiger classification [*Kottek et al.*, 2006] is reported to show that at least one site for each of the climatic regimes (with exception of regime E, polar climate) has been considered, in order to study as many precipitation forms and patterns as possible. Furthermore, on average, each data set covers a range of time of 1 year, including many types of events (i.e., stratiform, convective and orographic) (see Table 2). Note that two different types of disdrometer have been used: the JWD impact disdrometer and the THIES optical disdrometer [see *Joss and Waldvogel*, 1967; *Frasson et al.*, 2011; *Tokay et al.*, 2013 for instruments description].

It is noteworthy that disdrometers are affected by measurement errors, which in general cause underestimation of the rain totals [*Tokay and Short*, 1996; *Tokay et al.*, 2001]. Studies in the literature indicate that impact disdrometers may underestimate small drops [*Tokay et al.*, 2005], while optical disdrometer may overestimate the number of large drops in case of intense rainfall events [*Lanzinger et al.*, 2006]. The causes and the magnitude of these errors are different, according to the type of instrument used. The most relevant errors are: errors caused by the dead time minimum interval between two consecutive drops, which can be not enough sensitive (for impact disdrometers only); calibration errors, due to the discrepancy between the channel width specified by the vender and the effective one; wind related errors; acoustic noise from the surroundings. The last three types of errors can be reduced to a minimum by a proper installation of the instrument; these cautions have been used for all the considered sites.

Regarding the dead time errors, usually the so-called dead time correction is adopted. This was introduced, on the advice of A. Waldvogel, by *Sheppard and Joe* [1994] in order to limit the underestimation of small drops, caused by the use of JWD disdrometer. Note that many Authors have used this correction [i.e., *Sauvageot and Lacaux*, 1995; *Uijlenhoet et al.*, 2002; *Brawn and Upton*, 2008]. Many others [i.e., *Tokay and Short*, 1996; *Tokay et al.*, 2001; *Uijlenhoet et al.*, 2003] have chosen to not to implement it, for different reasons: (1) it modifies the DSD and increases the moments of the drop size, such as the rain rate, significantly, (2) it does not add drops if there are no drops in a given channel or simply, (3) it did not alter their findings. For sake of clarity, we have applied the dead time

Table 2. List of the Sites Where Disdrometer Data Are Collected With Starting Minute Date, Ending Minute Date, Number of Total Minutes, and Type of Instrument

Code	Starting Minute	Ending Minute	Total Minutes	Instrument
BKT	14 Aug 2001	30 Jul 2003	66,402	JWD
DRW	04 Nov 2005	10 Feb 2006	6863	JWD
ETO	18 Jul 2005	25 Sep 2005	1496	JWD
KSH	2 May 1979	24 Jul 1981	67,114	JWD
MIK	30 Apr 2003	31 Dec 2007	85,752	JWD
MAC	15 Sep 1999	06 Nov 1999	9530	JWD
MLN	15 Jul 2011	27 Dec 2012	34,696	THIES
TRN	1 Jan 2009	31 Dec 2009	27,587	THIES

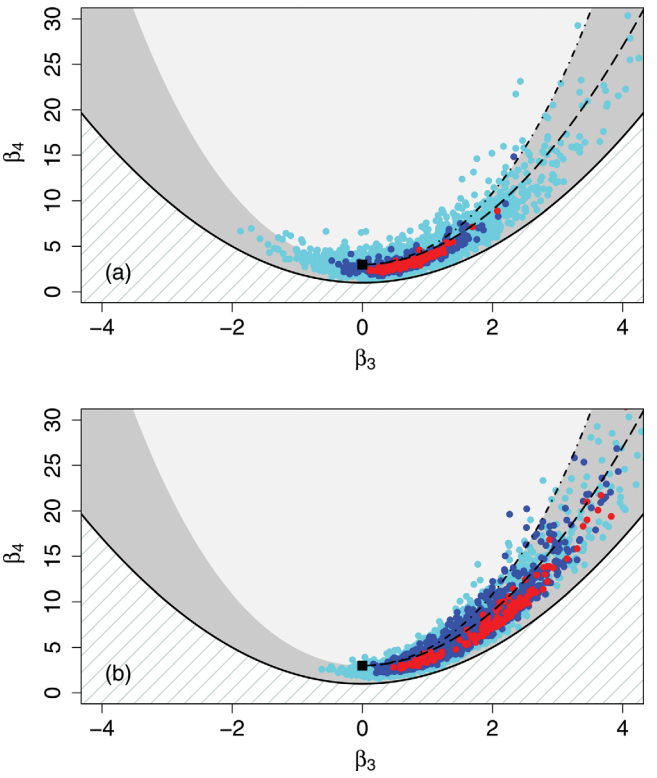

Figure 1. Skewness (β_3)-kurtosis (β_4) plane with sample values of 1 min data for (a) Darwin and (b) Milano. The Normal occupies the squared black point, the Lognormal (as the Johnson SL) the dash-dot curve, the Gamma the dashed curve, the Johnson SB the dark gray area, and the Johnson SU the light gray area. Different colors indicate different sample sizes: $N \leq 1000$ in cyan, $1000 < N < 2000$ in blue, and $N \geq 2000$ in red.

correction to JWD data. The results show that its application does not qualitatively change the conclusions of this paper (see supporting information for details). For this reason, we have decided to not to adopt this correction in the rest of the manuscript.

Furthermore, in order to minimize statistical sampling errors, we exclude minutes with a number of drops less than 60 and/or with number of occupied diameter classes less than 3.

The analyses reported in the next are focused on the original data sets, observed at 1 min time interval. In order to be as general as possible, we have extended the analyses to longer periods, by considering in particular 2, 3, and 5 min temporal aggregation (see Appendix C for details).

4. Skewness-Kurtosis Plane as Synoptic View

Let us indicate with β_r the rth statistical moment, defined as:

$$\beta_r = E\left[\left(\frac{X-\mu_X}{\sigma_X}\right)^r\right] \qquad (2)$$

where X is the random variable, $E[.]$ is the expected value, μ and σ are, respectively, the mean and the standard deviation [*Vargo et al.*, 2010]. We thus consider the skewness-kurtosis plane as the locus of the couples skewness, β_3, and kurtosis, β_4, (Figures 1–3). In the $\beta_3-\beta_4$ diagram, the limit curve, defined by $\beta_4-\beta_3^2-1\geq 0$, separates the theoretically impossible area (dashed area), by the portion of the plain that can be occupied by the pairs (β_3, β_4) of all distributions [*Pearson*, 1916]. Each distribution family occupies a specific portion of the skewness-kurtosis plane, that can be a point, as the Normal, a curve, as the Gamma and the Lognormal, or an area, as the Johnson SB and SU. In particular, the Johnson's system has a very important feature, it is designed to cover the whole skewness-kurtosis plane, thus it can match all the possible combinations of the two moments. This plane provides a synoptic view of the different behavior of the probability distributions and is sometimes used as a tool for the identification of the proper distribution for a given data set. However, its application can be problematic and difficult in the case of samples with limited length, where inaccurate statistical estimates occur. The candidate distributions are the

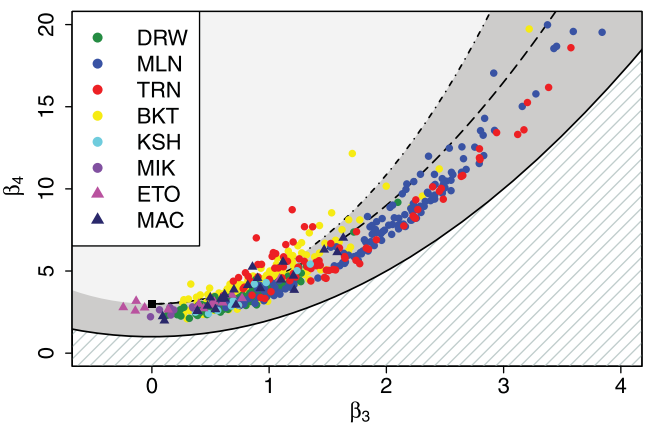

Figure 2. Skewness (β_3)-kurtosis (β_4) plane with sample values of 1 min data with $N \geq 2000$ for all the data sets, ($N \geq 1250$ for ETO and MAC). DRW green dots, MLN blue dots, TRN red dots, BKT yellow dots, KSH cyan dots, MIK purple dots, ETO magenta triangles, and MAC navy triangles.

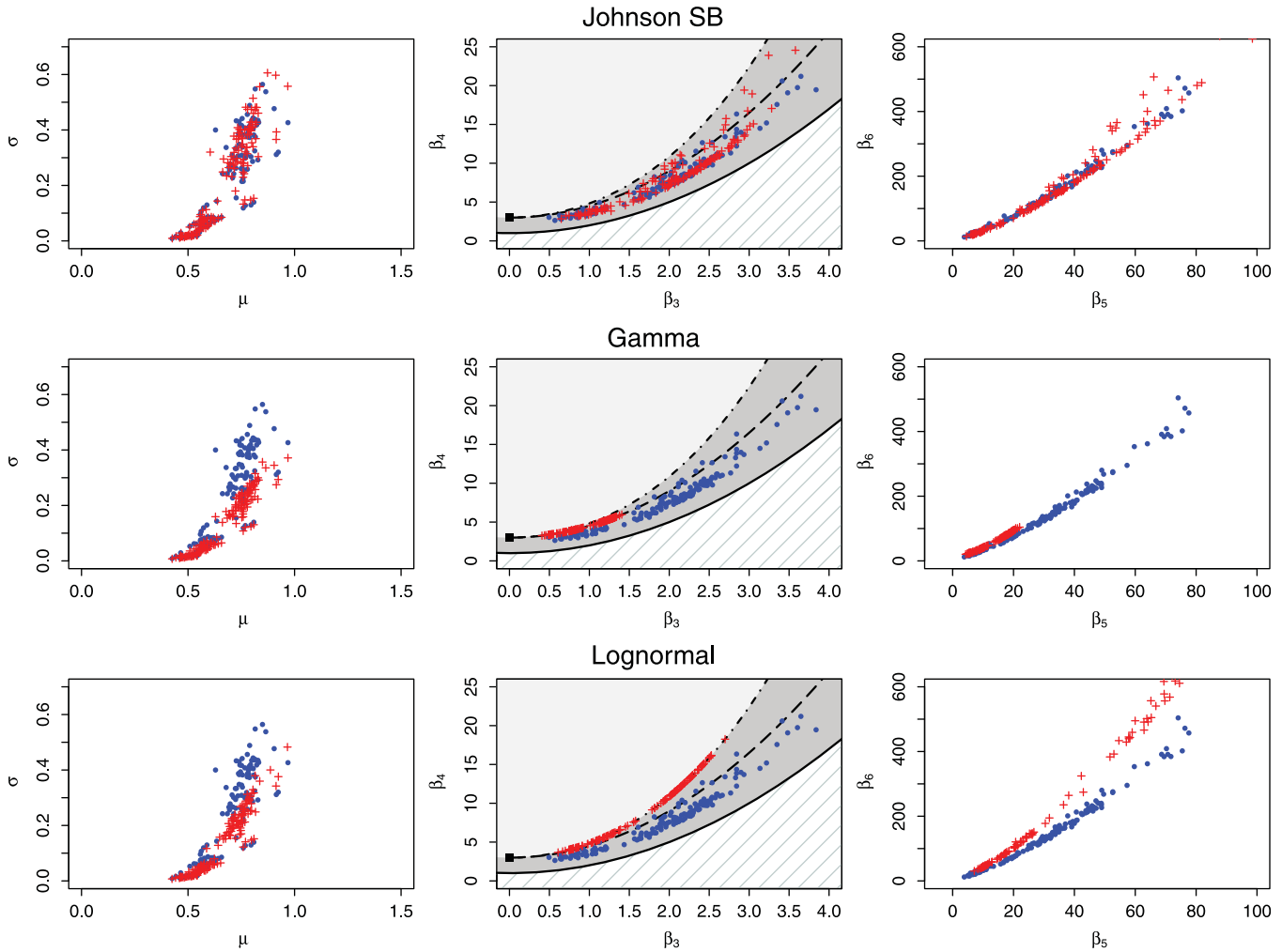

Figure 3. (left) Mean-variance diagrams, (middle) skewness-kurtosis, and (right) fifth moment-sixth moment for Milano with $N \geq 2000$. The blue dots are the empirical moments, while the red crosses are the theoretical moments calculated considering Johnson SB in the top row, Gamma in the medium and Lognormal in the bottom.

ones closer to the pairs (β_3, β_4) calculated empirically from data. It is interesting to note that the transformation of the variable $X \rightarrow \frac{X-\mu_X}{\sigma_X}$ does not alter skewness, kurtosis, and in general the rth statistical moment $E\left[\left(\frac{X-\mu_X}{\sigma_X}\right)^r\right]$. Thus, the renormalized drop diameter variable proposed by *Ignaccolo et al.* [2009] has the same couple (β_3, β_4) of the original variable. Consequently, this implies that the representation in the $\beta_3-\beta_4$ diagram does not vary if we consider rough or renormalized data.

A modified version of this plane has been already used by *Niu et al.* [2010] to investigate if the statistical pattern of the 1 min DSDs, measured by a Parsivel disdrometer located in Guyuan, followed the Gamma distribution. The modified moment ratio diagram has been obtained by calculating the deviation coefficients C_s and C_k, which represent the deviation in term of skewness and kurtosis from the classical Exponential distribution suggested by *Marshall and Palmer*, [1948]. For the Gamma distribution $C_s = C_k$, while for the exponential distribution $C_s = C_k = 1$. *Niu et al.* [2010] showed that the scatterplot of C_s and C_k calculated from the observed DSDs confirmed the deviation from the Exponential distribution, the points did not cluster around (1, 1). In our opinion however, it is impossible to state that the Gamma distribution well describes the data. In fact, (i) the scatterplot does not show the negative axes (the Gamma distribution does not admit negative values of C_s and C_k), while the cluster of the sample points seems to be cut by this limitation; (ii) the sample points move away from the Gamma line especially with the increase of C_s and C_k; (iii) the data set is site specific and is limited to 1 month precipitation data, (iv) only Gamma and Exponential distributions have been considered and plotted as reference line in the diagram.

Here three candidate distributions (Johnson SB, Gamma, and Lognormal) are used to match the empirical moments. In order to do this, for each data set, and each minute, we calculate the first six empirical moments (i.e., mean, standard deviation, β_3, β_4, β_5, and β_6) and we report the skewness and the kurtosis in the $\beta_3-\beta_4$ plane. The representation of the first six statistical moments gives an idea of the accuracy of the evaluation of the physical quantities, which are proportional to these moments. For example, the rainfall rate R is proportional to the third moment of the $p(D)$, while the reflectivity Z to the 6.67th moment. Figure 1 shows as example the sample values of skewness and kurtosis in the $\beta_3-\beta_4$ plane, distinguished by sample size, for Darwin (a) and Milano (b). Cyan dots represent minutes with $N \leq 1000$, blue dots $1000 < N < 2000$ and red dots $N \geq 2000$. The values are located principally in the SB domain (dark gray area). The ones outside the SB domain are usually characterized by smaller sample sizes, i.e., $N \leq 1000$, due to the difficulty of estimating high order moments with small samples. It is important to notice that quite all the couples characterized by $N \geq 2000$ stay under the Lognormal (dash-dot) and the Gamma (dashed) curves, see especially Milano (Figure 1b). Hence, the sample third and fourth moments do not fall in the domains of the distributions which are considered the best candidates for the statistical representation of raindrop size. Figure 2 reports the couples skewness-kurtosis of all the data sets, considering $N \geq 2000$, with exception of ETO and MAC that are characterized by minutes with smaller sample size. For these two data sets, we thus consider in these analyses a threshold sample size of 1250. With the exception of some points belonging mainly to Torino and Koto, all the couples occupy the Johnson SB sector and in particular, they stay in an area constantly below Gamma and Lognormal domains. In Figure 3, we report for Milano the moment-ratio diagrams mean-standard deviation, skewness-kurtosis, and β_5–β_6, comparing empirical (blue dots) and theoretical (red crosses) moments, for all the three distributions. It is easy to see that the correspondence is definitely better for the Johnson SB distribution. Similar results are obtained in the other data sets (see supporting information Figures S1–S7).

Finally, Figure 4 shows the histograms of the estimated four parameters of the Johnson SB distribution for Milano. The fill gray histograms are related to the entire data set, while the empty dashed red ones are related to the data set with $N \geq 2000$. Above each histogram, there is a box plot in which it is possible to distinguish the median value, the first and third percentiles and the outliers. Further studies are needed to evaluate the presence of dependence among parameters, for example, using statistical tools reported in *Salvadori et al*. [2007].

One problem affecting this analysis is in the fact that skewness and kurtosis are not bias-free, as stated by many authors [see e.g., *Bobee and Robiataille*, 1975]. In order to understand if this bias could effectively influence the outcomes we have proceeded as follows. First, we have estimated the bias of skewness and kurtosis following *Whiters and Nadarajah* [2011] and we have calculated unbiased skewness and kurtosis estimators according to their findings. The results have shown that the bias can be considered negligible. The location differences of the sample estimates in the moment-ratio diagram are almost unnoticeable. Second, we have alternatively made the analysis using the L-Moment Ratio Diagram (namely, L-skewness-L-kurtosis diagram), which confirms what we have already seen in the skewness-kurtosis diagram. These results are not reported here for brevity.

5. Model Selection

Here we have used two indices, the Akaike Information Criterion (AIC) and the Bayesian Information Criterion (BIC), to rank Johnson SB, Gamma and Lognormal, according to their ability in fitting 1 min DSDs. AIC and BIC indices are defined as:

$$AIC = 2k - 2L^* \tag{3}$$

$$BIC = k\ \ln(N) - 2L^* \tag{4}$$

where k is the number of parameters in the model and L^* the maximized value of the log-likelihood. These two indices have been developed starting from two different ideas. According to [*Wagenmakers and Farrell*, 2004], "*... the BIC assumes that the true generation model is in the set of candidate models, and it measures the degree of belief that a certain model is the true data-generating model. The AIC does not assume that any of the candidate models is necessarily true, but rather calculates for each model a measure of distance between the probability density generated by the model and reality*." Furthermore, the two indices differ in the way the

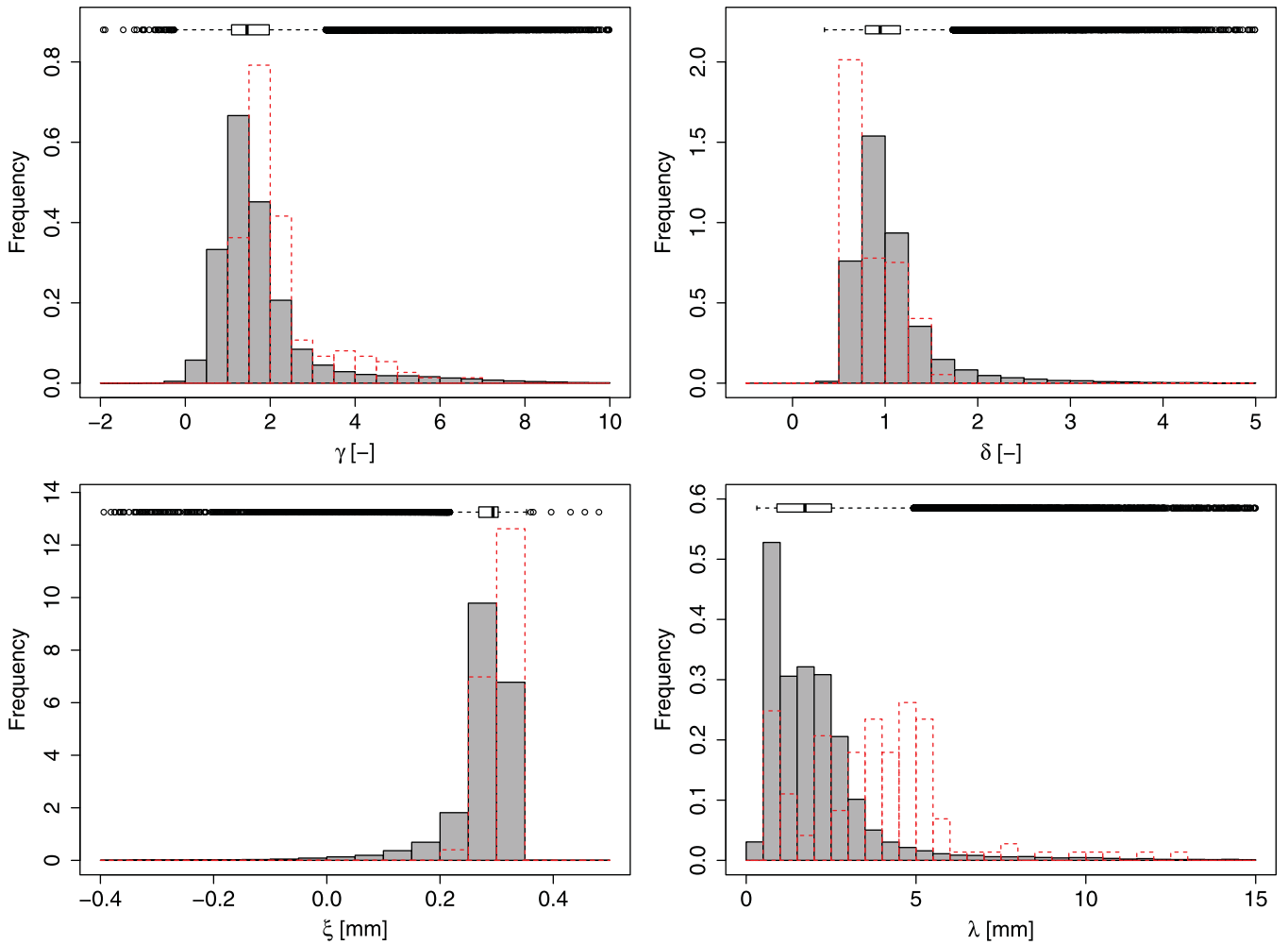

Figure 4. Frequency histograms of the four parameters of Johnson SB. The entire MLN data set (fill gray histogram) and the minutes with $N \geq 2000$ (empty dashed red histogram).

number of free parameters is considered. For AIC the penalization function is constant, for BIC it depends on the logarithm of the number of observations. Thus, at relatively low N (10 and less) BIC is more tolerant of free parameters than AIC, but less tolerant at higher N (as the natural log of N overcomes 2). Since there is no consensus on the choice on the index to use, we have decided to report the results of both the two indices, which are consistent, making us confident in the results obtained. For both AIC and BIC, the chosen model is the one that minimizes the values of the index. Actually, the selection of the model through the individuation of the minimum AIC is not certain, especially if the sample size is small [*Akaike*, 1974]. A correction in the estimation of AIC for finite sample size, namely the corrected AIC, AICc, has been introduced by *Sugiura* [1978]. The use of AIC and AICc criteria produces almost equal outcomes. For this reason AICc results are not reported here.

Table 3 gives the results for Darwin and Milano data sets: for each distribution the number of times the model is selected is reported in percentage. For example, considering AIC index and the whole MLN (DRW) data set, Johnson SB is the best candidate distribution for 88% (69%), against 5% (14%) for Gamma and 8% (17%) for Lognormal. Considering BIC, the percentages are less advantageous for Johnson SB because BIC is more sensitive to the number of parameters. In case, we consider only the minutes with $N \geq 2000$, the results are almost totally in favor of Johnson SB for both MLN and DRW data sets and both the indices. Same results are obtained also for the other six data sets (see supporting information Table S1).

Furthermore, it can be useful to take into account the absolute differences between AIC (or BIC) values calculated for the three distributions and each sample: small differences, in the order of some units, make the

Table 3. (Top) Percentage of the Number of Times a Model Is Selected According to (Left) AIC and (Right) BIC for DRW and MLN, Considering the Entire Data Set and Only the Minutes With $N \geq 2000$[a]; (Bottom) Percentage of Acceptance of the K-S Test Using the (Left) Standard Method and (Right) the Keutelian Method (Right) for the Same Data Sets

	AIC			BIC		
Data Set	Johnson SB	Gamma	Lognormal	Johnson SB	Gamma	Lognormal
DRW	69	14	17	46	25	29
MLN	90	4	6	77	7	16
DRW ($N \geq 2000$)	99	0	1	97	1	2
MLN ($N \geq 2000$)	100	0	0	100	0	0
	Standard method			Keutelian method		
	Johnson SB	Gamma	Lognormal	Johnson SB	Gamma	Lognormal
DRW	91	77	75	66	52	51
MLN	91	73	81	66	41	52
DRW ($N \geq 2000$)	78	22	14	32	3	1
MLN ($N \geq 2000$)	47	0	0	12	0	0

selection of the model uncertain. Let the AIC values be denoted as AIC_J if referred to Johnson SB, AIC_G to Gamma, AIC_L to Lognormal, and $AIC_{\min}$ the minimum value. Then, the relative likelihood is defined as $\exp\left((AIC_{\min} - AIC_i)/2\right)$, with $i = J, G, L$, and can be interpreted as the relative probability of the ith model respect to the one having minimum AIC. If this probability is small, the selection of the model with smaller AIC can be considered accurate. For example, if we consider a $(AIC_{\min} - AIC_i)$ threshold value of 6 units, the probability that the ith model is as probable as the one with $AIC_{\min}$, is around 0.05. At this point, we can proceed as follows. We consider the minutes in which the Johnson SB, having $AIC_{\min}$, is selected and calculate the percentage of minutes in which the relative AIC differences with the other distributions is less than 6. For the data set of Darwin ($N \geq 2000$) and for the 69% of the minutes for which Johnson SB is selected, the percentage of minutes in which the difference $AIC_J - AIC_G$ ($AIC_J - AIC_L$) is less than 6 is 22% (24%). For the data set of Milan ($N \geq 2000$) and for the 90% of the minutes for which Johnson SB is selected, the percentage of minutes in which the absolute difference $AIC_J - AIC_G$ ($AIC_J - AIC_L$) is less than 6 is 6% (12%). Given these low percentages, it is possible to state that the selection of the Johnson SB model with the use of AIC is accurate for the great majority of the cases. In addition, we can also calculate the percentages of minutes in which Gamma (Lognormal) is selected, but for which the absolute difference $AIC_G - AIC_J$ ($AIC_L - AIC_J$) is less than 6. The percentages are indeed very high reaching 98% (99%) for the data set of Darwin and 96% (99%) for the data set of Milan, showing a great uncertainty in the selection of Gamma and Lognormal distributions and attesting the Johnson SB as a valid alternative candidate. The same analysis has been carried out considering BIC values, similar results have been obtained. Thus, AIC and BIC confirm what was already found using the $\beta_3 - \beta_4$ plane.

6. Model Testing

Finally, we have considered the Kolmogorov-Smirnov (K-S) goodness-of-fit test to check the agreement between a probability distribution and data. Even if AIC and BIC indices have selected the Johnson SB for the majority of cases in all databases, we have applied this test to each of the three distributions. The K-S test compares the cumulative frequency with the cumulative probability distribution. The K-S test statistic is the maximum distance, in absolute value, between cumulative frequency and cumulative distribution. If none of the parameters are estimated from the data, the test statistic has a limiting distribution, independent on the distribution under analysis. In this case (indicated in the next as standard), the critical value is easily calculated according to the significance level (α) and the sample size (N). If $N > 35$ and $\alpha = 0.01$, the critical value is $1.6276/\sqrt{N}$. If the parameters are estimated from the data, the distribution of the test statistic is dependent on the distribution under analysis, and the critical value must be calculated ad hoc. We have made this calculation following the procedure proposed by Keutelian, [*Keutelian*, 1991; *Ignaccolo and De Michele*, 2013]. It consists in the estimation of the critical value of the test statistic by the use of Monte-Carlo simulations. For each distribution and each minute, the parameters have been estimated with the ML method. These parameters have been used for the generation of 10,000 samples (for each minute) with

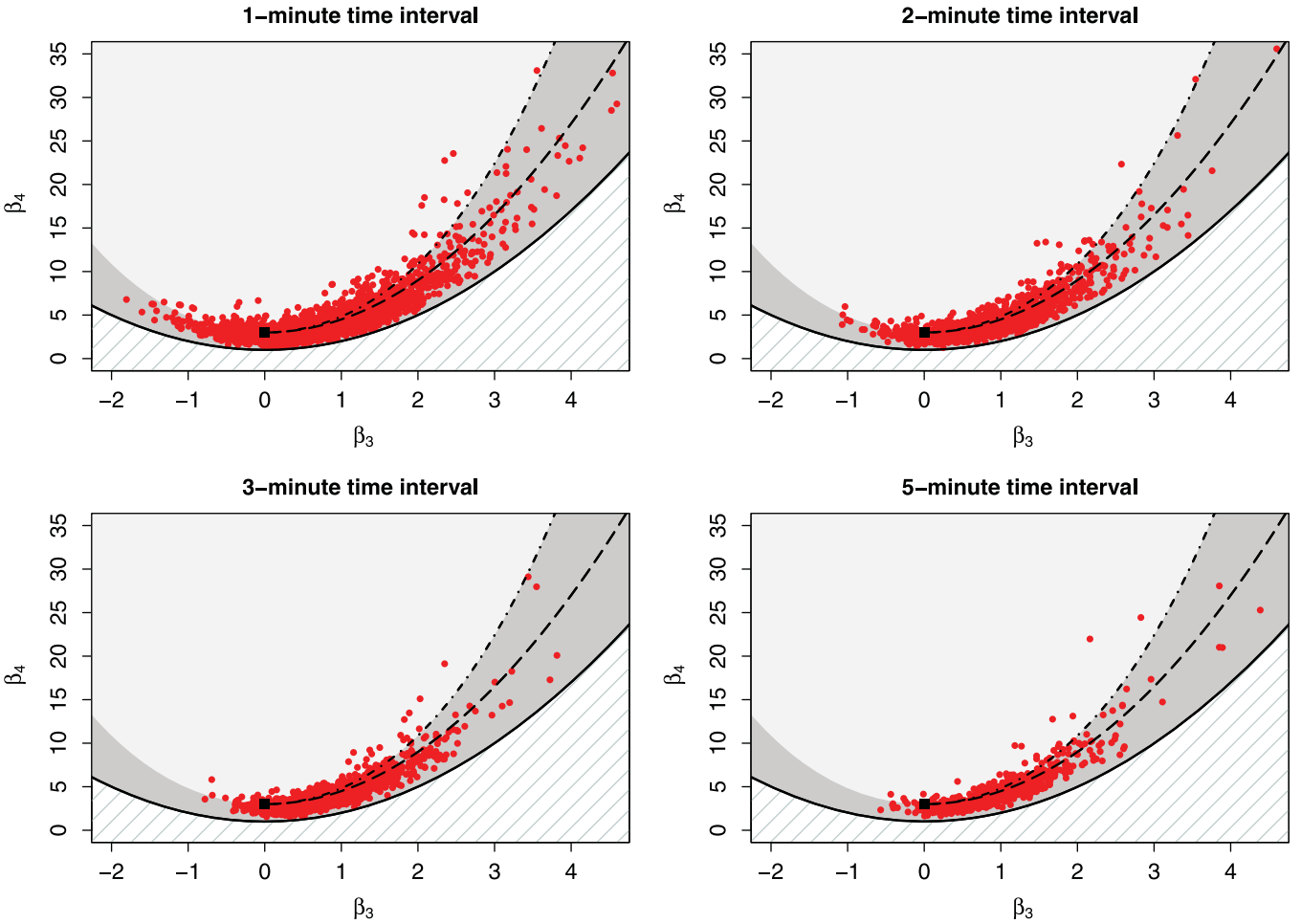

Figure 5. Skewness (β_3)-kurtosis (β_4) plane with sample values of Darwin data set with 1, 2, 3, and 5 min time interval.

length equal to the length of the considered sample minute. The parameters have been reestimated for each of the 10,000 samples and the maximum difference, D_{crit}, between the cumulative distribution function and the cumulative frequencies computed. The critical value of the test statistic is the 99% percentile, D_{crit_99}. The test is accepted if the maximum difference in absolute value, D, between the theoretical cumulative distribution and the cumulative frequency of the observed sample minute is smaller than D_{crit_99}.

The K-S goodness-of-fit test with a 1% level of significance is applied to each data set, considering both the standard procedure and the one suggested by *Keutelian* [1991]. Table 3 shows the results in terms of percentages of acceptance of each of the three distributions, for Darwin and Milano, considering all minutes, or only those with $N \geq 2000$. At first, it is easy to see that the percentages of acceptance decrease passing from standard to Keutelian procedure. The comparison of the three distributions shows that Johnson SB is always the choice which ensures the better result, regardless of the data set and the method used. If we consider the data sets with $N \geq 2000$, for Darwin and the Keutelian (standard) procedure, Johnson SB has a percentage of acceptance of 32% (78%), Gamma 3% (22%), Lognormal 1% (14%). For Milano, the percentages are even worse: Johnson SB has a percentage of

Table 4. Percentages of the Number of Times a Model Is Selected According to AIC and BIC for DRW Data Set, Considering 1, 2, 3, and 5 Min Time Intervals

	Johnson SB	Gamma	Lognormal	
AIC	69	14	17	1 min
BIC	46	25	29	
AIC	78	10	12	2 min
BIC	55	20	25	
AIC	88	5	7	3 min
BIC	71	12	17	
AIC	94	0	3	5 min
BIC	96	0	4	

acceptance of 12% (47%), while Gamma and Lognormal are rejected at all. Similar percentages of acceptance/rejection have been found for the other data sets (see supporting information Table S2). For $N \geq 2000$, the percentages of acceptance of Johnson SB are better than the other two distributions, but low however. This can be explained by the fact that the K-S test is applied to data sets with a very large sample size, thus the differences between the theoretical and the empirical distributions are very small and the test tends to be quite restrictive. Despite of it, Johnson SB obtains a considerable percentage of acceptance. Conversely, when the sample size is small, less than about 100 [*Kottegoda and Rosso*, 2008], the random fluctuations influence the K-S test in a way that it tends to pass for almost all the three distributions, and so the test becomes less significant. Thus, for all the three distributions, with the increase of the sample size we register a decrease of the percentages of acceptance, but these values decrease to reach almost zero in case of Gamma and Lognormal, unlike the case of Johnson SB.

Plots comparing the three density functions (with parameters estimated through ML method) and the histogram of 1 min disdrometer data and q-q plots (probability plot comparing sample and theoretical quantiles) contribute to make clear the results of the statistical analyses (see also supporting information, Figures S8–S15.)

7. Conclusions

Eight data sets of 1 min disdrometer data collected at different locations in the world have been considered to investigate extensively the drop size distribution of rainfall. Gamma and Lognormal, the most widely used distributions for the representation of DSDs, together with our proposal, the Johnson SB, have been fitted to the data (with different temporal aggregations) and statistically compared. Even if Gamma and Lognormal are simple and useful approximations of observed DSD spectra, our analyses show that they do not seem to be enough accurate in the statistical representation of the drop diameter variability, with also a physical argument.

Physically, this inadequacy stems from the fact that Gamma and Lognormal are upper unbounded, where the drop diameter is both lower and upper bounded as the Johnson SB. Besides that, this last distribution has been adopted in a recent precipitation-related study, to describe the early time stage of evolution of drops due to coagulation phenomenon [*Tang and Lin*, 2013]. Clearly, there is not an established connection between the distribution of drops in the clouds due to coagulation and the distribution of drops at the ground. However, the fact that Johnson SB could represent both the two phenomena is intriguing and will be the subject of future investigations.

Statistically speaking, Gamma and Lognormal are inadequate to capture the variability of high order moments, unlike the Johnson SB. This is confirmed by the model selection analysis made through AIC and BIC indices and the goodness-of-fit check through the K-S test.

In conclusions, the statistical analyses presented suggest the Johnson SB as a general functional form for the description of the drop diameter variability at 1 min or larger (say 1–5 min) time intervals. Additional analyses are still necessary to support our achievement and plug it in practical applications.

Appendix A: The Johnson's System of Distributions

The Johnson's system of distributions was derived by *Johnson* [1949], in order to find a general and flexible model, which could cover a wide variety of shapes. This system is based on a transformed normal variate and it is composed by three families, SB, SU, and SL, so that any data set with finite moments can be fitted by one of them. If Z is a standardized normal variate (zero mean, standard deviation equal to 1), X a continuous random variate, being $Y = \frac{X-\xi}{\lambda}$, the system can be defined by:

$$Z = \gamma + \delta f(Y) \tag{A1}$$

where f is the transformation function, γ and δ are the shape parameters, λ is the scale parameter, and ξ is the location parameter, with $\delta > 0$ and $\lambda > 0$. Three normalizing transformations has been defined, see *Johnson* [1949] and *George and Ramachandran* [2011].

The Lognormal system of distribution, SL, which covers the Lognormal family and is defined by:

$$Z = \gamma + \delta \ \ln\left(\frac{X-\xi}{\lambda}\right),\ X > \xi \tag{A2}$$

The bounded system of distribution, SB, which can be upper or lower bounded or both. It covers Gamma, Beta and also other distributions; it is defined by:

$$Z = \gamma + \delta \ \ln\left(\frac{X-\xi}{\xi+\lambda-X}\right),\ \xi < X < \xi+\lambda \tag{A3}$$

The unbounded system of distribution, SU, covering the Normal and T distributions above all and being defined by:

$$Z = \gamma + \delta \ \ln\left[\left(\frac{X-\xi}{\lambda}\right)+\left\{\left(\frac{X-\xi}{\lambda}\right)^2+1\right\}^{1/2}\right],\ -\infty < X < \infty \tag{A4}$$

Thanks to these transformations, Z follows a standard Normal distribution, while X follows the Johnson distribution.

In the next, we focus the attention to Johnson SB. The cumulative distribution function of the Johnson SB is not available in a closed form, but can be expressed through the Normal distribution as:

$$F(x) = \Phi\left[\gamma+\delta \ \ln\left(\frac{x-\xi}{\lambda+\xi-x}\right)\right] \tag{A5}$$

where Φ is the standard cumulative Normal function.

The quantile with fixed level of probability α, x_α, is calculated as:

$$x_\alpha = \xi+\lambda\left[1+\exp\left(\frac{\gamma-\Phi^{-1}(\alpha)}{\delta}\right)\right]^{-1} \tag{A6}$$

where Φ^{-1} is the inverse of Φ.

The rth statistical moment around zero, μ'_r, of Johnson SB is a transcendental quantity not so easy to calculate,

$$\mu'_r = \frac{1}{\sqrt{2\pi}}\int_{-\infty}^{\infty} e^{-\frac{1}{2}z^2}(1+\exp(-(z-\gamma)/\delta))^{-r}dz \qquad r=1,2,\ldots \tag{A7}$$

where z is a unit normal variable. *Johnson* [1949] proposed a method for the estimation of the first four moments around 0. At first, an algebraic simplified formula of μ'_1 has been derived starting from the general μ'_r integral. Then, the higher moments μ'_2, μ'_3, and μ'_4 can be expressed in terms of the partial derivatives of the μ'_1 with respect to the parameter γ. Alternatively, a recurrence formula, which emphasizes the dependence of μ'_k on γ and δ, has also been derived. Through its use, it is possible to evaluate the first four noncentral moments. The passage between raw and central moments can be easily done [see e.g., *Kottegoda and Rosso*, 2008].

In this work the central moments, β_r, of the Johnson SB distribution are calculated numerically using a Monte Carlo approach.

Appendix B: Maximum Likelihood Parameters Estimation

We use the Maximum Likelihood (ML) method to estimate the parameters of the Johnson SB, Gamma and Lognormal. Regarding Gamma and Lognormal, the ML estimation of the parameters is implemented through the use of the R package "*MASS*" and the function *fitdistr* [see *Venables and Ripley*, 2002]. The same package is also used to calculate the six central moments which are necessary to obtain the couples of the mean-variance, skewness-kurtosis, and β_5–β_6 planes. The ML parameters estimation for the Johnson SB is trickier, because a function like the previous one concerning this distribution is not available until now. The

problem is solved as follows. Starting from the density function of the Johnson SB, equation (1), the log-likelihood function can be written as:

$$L^* = N\ln(\lambda) + N\ln(\delta) + N\ln(2\pi)^{-1/2} - N\gamma^2/2 - \sum \ln(x_i - \xi) - \sum \ln(\xi + \lambda - x_i) - \gamma\delta \sum \ln(x_i - \xi) + \gamma\delta \sum \ln(\xi + \lambda - x_i) - (\delta^2/2) \sum [\ln(x_i - \xi) - \ln(\xi + \lambda - x_i)]^2 \quad \text{(B1)}$$

where $\sum$ stands for $\sum_{i=1}^{N}$ and N is the number of observations in the data set. Taking the partial derivatives respect to the parameters and equating these to zero, a system of four equations is obtained [see *Kottegoda*, 1987]. In practice the R function *optim* has been adopted, with the assumption of specified initial values (ξ_{start} and λ_{start}). Being the Johnson SB a bounded distribution in the interval $[\xi, \xi+\lambda]$ and being the DSDs physically bounded below and above by the minimum and maximum drops diameter, D_{min} and D_{max}, the initial values of ξ and λ are chosen sufficiently below and above the lowest and the highest sample observations, respectively. Thus, ξ_{start} is set equal to $(D_{min} - \varepsilon_1)$ and λ_{start} is set equal to $(D_{max} - \xi_{start} + \varepsilon_2)$, where ε_1 and ε_2 are two arbitrarily small quantities.

Appendix C: Analyses at 2, 3, and 5 Min Temporal Aggregation

With the aim of proving the generality of the proposed Johnson SB model, we have made the analysis of disdrometer data observed at longer time intervals, in particular 2, 3, and 5 min temporal aggregations. We do not go beyond 5 min in order to group together data with the same mean and variance, following *Ignaccolo and De Michele* [2010]. Figure 5 shows the skewness-kurtosis plane (the red dots represent the $(\beta_3$–$\beta_4)$ couples) for the data sets of Darwin (AM climate). In the figure, there are four plots related to the four aggregation time intervals (1, 2, 3, and 5 min). The comparison between the plots shows that the increase of the aggregation time does not generally affect the location of the cloud of points in the $(\beta_3$–$\beta_4)$ plane. The dots are mainly located in the Johnson SB domain and the percentage of dots inside this area increases with the increase of the aggregation time.

The evaluation of the AIC and BIC indices confirms the outcomes of the skewness-kurtosis plane (see Table 4 related to the data sets of Darwin). For each distribution and each aggregation time, the number of times the model is selected is reported in percentage, considering both the raw data sets and the data sets with dead time correction. The table shows that the higher the aggregation time, the higher the Johnson SB percentage is.

Similar results have been obtained with the other seven data sets (both raw and dead time corrected), demonstrating the potentiality of the Johnson SB distribution, which is able to outperform the other two considered models (namely Gamma and Lognormal) even across different time scales.

Acknowledgments

We wish to thank C. R. Williams and the National Oceanic and Atmospheric Administration (public availability of the data set recorded at Darwin and Kwajalein), the National Institute of Information and Communication Technology, Japan (Kashima data set), the Institute of Observational Research for Global Change together with the Japan Agency for Marine-Earth Science and Technology (Bukit Koto Tabang data set), the Environmental Protection Agency of Piemonte, Italy (Torino data set). Data are available at the URL: http://ecohys.blogspot.it/p/data.html. We also thank the Associate Editor and the Anonymous Reviewers for the useful comments.

References

Akaike, H. (1974), A new look at the statistical model identification, *IEEE Trans. Autom. Control*, *19*(6), 716–723, doi:10.1109/TAC.1974.1100705.

Bobee, B., and R. Robiataille (1975), Correction of bias in the estimation of the coefficient of skewness, *Water Resour. Res.*, *11*(6), 851–854, doi:10.1029/WR011i006p00851.

Brawn, D., and G. Upton (2008), Estimation of an atmospheric Gamma drop size distribution using disdrometer data, *Atmos. Res.*, *87*(1), 66–79, doi:10.1016/j.atmosres.2007.07.006.

Bringi, V. N., V. Chandrasekar, J. Hubbert, E. Gorgucci, W. L. Randeu, and M. Schoenhuber, (2003), Raindrop size distribution in different climatic regimes from disdrometer and dual-polarized radar analysis, *J. Atmos. Sci.*, *60*(2), 354–365, doi:10.1175/1520-0469(2003)060<0354:RSDIDC>2.0.CO;2.

Cataneo, R., and G. E. Stout (1968), Raindrop-size distributions in humid continental climates, and associated rainfall rate-radar reflectivity relationships, *J. Appl. Meteorol.*, *7*(5), 901–907, doi:10.1175/1520-0450(1968)007<0901:RSDIHC>2.0.CO;2.

De Michele, C., and M. Ignaccolo (2013), New perspectives on rainfall from a discrete view, *Hydrol. Processes*, *27*, 2379–2382, doi:10.1002/hyp.9782.

Feingold, G., and Z. Levin (1986), The Lognormal fit to raindrop spectra from frontal convective clouds in Israel, *J. Clim. Appl. Meteorol.*, *25*(10), 1346–1363, doi:10.1175/1520-0450(1986)025<1346:TLFTRS>2.0.CO;2.

Frasson, R. P. M., L. K. Cunha, and W. K. Krajewski (2011), Assessment of the Thies optical disdrometer performance, *Atmos. Res.*, *101*(1), 237–255, doi:10.1016/j.atmosres.2011.02.014.

Fujiwara, M. (1965), Raindrop-size distribution from individual storms, *J. Atmos. Sci.*, *22*(5), 585–591, doi:10.1175/1520-0469(1965)022<0585:RSDFIS>2.0.CO;2.

George, F., and K. M. Ramachandran (2011), Estimation of parameters of Johnson's system of distributions, *J. Mod. Appl. Stat. Methods*, *10*(2), 494–504.

Ignaccolo, M., and C. De Michele (2010), Statistical collapse of stratiform and convective drop diameter distributions at the ground, *Geophys. Res. Lett.*, *37*, L24402, doi:10.1029/2010GL045454.

Ignaccolo, M., and C. De Michele (2011), The discrete charm of rain, *Phys. Today*, *64*(1), 68–69, doi:10.1063/1.3541954.

Ignaccolo, M., and C. De Michele (2013), Phase space parameterization of rain: The inadequacy of Gamma distribution, *J. Appl. Meteorol.*, *53*(2), 548–562, doi:10.1175/JAMC-D-13–050.1.
Ignaccolo, M., C. De Michele, and S. Bianco (2009), The drop-like nature of rain and its invariant statistical properties, *J. Hydrometeorol.*, *10*, 79–95, doi:10.1175/2008JHM975.1.
Illingworth, A. J., and T. M. Blackman (2002), The need to represent raindrop size spectra as normalized Gamma distributions for the interpretation of polarization radar observations, *J. Appl. Meteorol.*, *41*(3), 286–297, doi:10.1175/1520-0450(2002)041<0286:TNTRRS>2.0.CO;2.
Ishii, S., S. Sayama, and T. Kamei (2011), Measurement of rain attenuation in terahertz wave range, *Wireless Eng. Technol.*, *2*, 119–124, doi:10.4236/wet.2011.23017.
Jaffrain, J., A. Studzinski, and A. Berne (2011), A network of disdrometers to quantify the small-scale variability of the raindrop size distribution, *Water Resour. Res.*, *47*, W00H06, doi:10.1029/2010WR009872.
Jameson, A. R., and A. B. Kostinski (2001), What is a raindrop size distribution?, *Bull. Am. Meteorol. Soc.*, *82*(6), 1169–1177, doi:10.1175/1520-0477(2001)082<1169:WIARSD>2.3.CO;2.
Jiang, H., M. Sano, and M. Sekine (1997), Weibull raindrop-size distribution and its application to rain attenuation, *IEEE Proc. Microwaves Antennas Propag.*, *144*(3), 197–200, doi:10.1049/ip-map:19971193.
Johnson, N. L. (1949), System of frequency curves generated by method of translation, *Biometrika*, *36*, 149–176.
Joss, J., and E. G. Gori (1978), Shapes of raindrop size distributions, *J. Appl. Meteorol.*, *17*(7), 1054–1061, doi:10.1175/1520-0450(1978)017<1054:SORSD>2.0.CO;2.
Joss, J., and A. Waldvogel (1967), Ein Spektrograph fur Niederschlagstropfen mit automatischer Auswertung, *Pure Appl. Geophys.*, *68*, 240–246, doi:10.1007/BF00874898.
Keutelian, H. (1991), The Kolmogorov-Smirnov test when parameters are estimated from data, *CDF Note 1285*, 13 pp., Fermilab, U.S. Dep. of Energy, Washington, D. C.
Kostinski, A. B., and A. R. Jameson (1999), Fluctuation properties of precipitation. Part iii: On the ubiquity and emergence of the Exponential drop size spectra, *J. Atmos. Sci.*, *56*(1), 111–121, doi:10.1175/1520-0469(1999)056<0111:FPOPPI>2.0.CO;2.
Kottegoda, N. T. (1987), Fitting Johnson SB curve by the method of maximum likelihood to annual maximum daily rainfalls, *Water Resour. Res.*, *23*(4), 728–732 doi:10.1029/WR023i004p00728.
Kottegoda, N. T., and R. Rosso (2008), *Applied Statistics for Civil and Environmental Engineers*, 2nd ed., Blackwell Publ., Oxford, U. K.
Kottek, M., J. Grieser, C. Beck, B. Rudolf, and F. Rubel (2006), World map of the Köppen-Geiger climate classification updated, *Meteorol. Z.*, *15*(3), 259–263, doi:10.1127/0941–2948/2006/0130.
Kotz, S., and J. R. Van Dorp (2004), *Beyond Beta: Other Continuous Families of Distributions with Bounded Support and Applications*, World Sci., Singapore.
Kumar, L. S., Y. H. Lee, and J. T. Ong (2011), Two-parameter Gamma drop size distribution models for Singapore, *IEEE Trans. Geosci. Remote Sens.*, *49*(9), 3371–3380, doi:10.1109/TGRS.2011.2124464.
Lanzinger, E., M. Theel and H. Windolph (2006), Rainfall amount and intensity measured by the Thies laser precipitation monitor, in *TECO-2006*, *Geneva*, *Switzerland*, session *3*, vol. 3, pp. 4–6.
Laws, J. O., and D. A. Parsons (1943), The relation of raindrop-size to intensity, *Trans. AGU*, *24*, 452–460, doi:10.1029/TR024i002p00452.
Lee, G. W., I. Zawadzki, W. Szyrmer, D. Sempere-Torres, and R. Uijlenhoet (2004), A general approach to double-moment normalization of drop size distributions, *J. Appl. Meteorol.*, *43*(2), 264–281, doi:10.1175/1520-0450(2004)043<0264:AGATDN>2.0.CO;2.
Marshall, J. S., and W. M. Palmer (1948), The distribution of raindrops with size, *J. Meteorol.*, *5*, 165–166, doi:10.1175/1520-0469(1948)005<0165:TDORWS>2.0.CO;2.
Niu, S., X. Jia, J. Sang, X. Liu, C. Lu, and Y. Liu (2010), *J. Appl. Meteorol. Climatol.*, *49*(4), 632–645, doi:10.1175/2009JAMC2208.1.
Norman, M. J. T., C. J. Pearson, and P. G. E. Searle (1995), *The Ecology of Tropical Food Crops*, Cambridge Univ. Press, Cambridge, U. K.
Owolawi, P. (2011), Raindrop size distribution model for the prediction of rain attenuation in Durban, *PIERS Online*, *7*, 516–523.
Pearson, K. (1916), Mathematical contributions to the theory of evolution. xix. Second supplement to a memoir on skew variation, *Philos. Trans. R. Soc. London A*, *216*, 429–457, doi:10.1098/rsta.1916.0009.
Pruppacher, H. R., and J. D. Klett (2010), *Microphysics of Clouds and Precipitation*, Springer, N. Y.
Rennolls, K., and M. Wang (2005), A new parameterization of Johnson's SB distribution with application to fitting forest tree diameter data, *Can. J. For. Res.*, *35*, 575–579, doi:10.1139/X05–006.
Rosenfeld, D., and C. W. Ulbrich (2003), Cloud microphysical properties, processes, and rainfall estimation opportunities, *Meteorol. Monogr.*, *30*(52), 237–237, doi:10.1175/0065–9401(2003)030<0237:CMPPAR>2.0.CO;2.
Salvadori, G., C. De Michele, N. Kottegoda, and R. Rosso (2007), *Extremes in Nature: An Approach Using Copulas*, Springer, Berlin.
Sauvageot, H., and J.-P. Lacaux (1995), The shape of averaged drop size distributions, *J. Atmos. Sci.*, *52*(8), 1070–1083, doi:10.1175/1520-0469(1995)052<1070:TSOADS>2.0.CO;2.
Sekhon, R. S., and R. C. Srivastava (1971), Doppler radar observations of drop-size distributions in a thunderstorm, *J. Atmos. Sci.*, *28*(6), 983–994, doi:10.1175/1520-0469(1971)028<0983:DROODS>2.0.CO;2.
Sekine, M., S. Ishii, S. I. Hwang, and S. Sayama (2007), Weibull raindrop-size distribution and its application to rain attenuation from 30 GHz to 1000 GHz, *Int. J. Infrared Millimeter Waves*, *28*(5), 383–392, doi:10.1007/s10762-007-9221-0.
Sempere Torres, D., J. M. Porrà, and J.-D. Creutin (1994), A general formulation for raindrop size distribution, *J. Appl. Meteorol.*, *33*(12), 1494–1502, doi:10.1175/1520-0450(1994)033<1494:AGFFRS>2.0.CO;2.
Sheppard, B. E., and P. I. Joe (1994), Comparison of raindrop size distribution measurements by a Joss-Waldvogel disdrometer, a PMS 2DG spectrometer, and a POSS Doppler radar, *J. Atmos. Oceanic Technol.*, *11*(4), 874–887.
Smith, J. A., E. Hui, M. Steiner, M. L. Baeck, W. F. Krajewski, and A. A. Ntelekos (2009), Variability of rainfall rate and raindrop size distributions in heavy rain, *Water Resour. Res.*, *45*, W04430, doi:10.1029/2008WR006840.
Spanos, A. (1999), *Probability Theory and Statistical Inference: Econometric Modeling With Observational Data*, Cambridge Univ. Press, Cambridge, U. K.
Strangeways, I. (2011), *Precipitation. Theory, Measurement and Distribution*, Cambridge Univ. Press, Cambridge, U. K.
Sugiura, N. (1978), Further analysts of the data by Akaike's information criterion and the finite corrections, *Commun. Stat.*, *7*(1), 13–26, doi:10.1080/03610927808827599.
Tang, H., and J. Lin (2013), Early-stage evolution of particle size distribution with Johnson's SB function due to Brownian coagulation, *Phys. Scr.*, *87*(5), 055401, doi:10.1088/0031–8949/87/05/055401.
Testud, J., S. Oury, R. A., Black, P. Amayenc, and X. Dou (2001), The concept of normalized distribution to describe raindrop spectra: A tool for cloud physics and cloud remote sensing, *J. Appl. Meteorol.*, *40*(6), 1118–1140, doi:10.1175/1520-0450(2001)040<1118:TCONDT>2.0.CO;2.

Tokay, A., and D. A. Short (1996), Evidence from tropical raindrop spectra of the origin of rain from stratiform versus convective clouds, *J. Appl. Meteorol.*, *35*(3), 355–371, doi:10.1175/1520-0450(1996)035<0355:EFTRSO>2.0.CO;2.

Tokay, A., A. Kruger, and W. F. Krajewski (2001), Comparison of drop size distribution measurements by impact and optical disdrometers, *J. Appl. Meteorol.*, *40*(11), 2083–2097, doi:10.1175/1520-0450(2001)040<2083:CODSDM>2.0.CO;2.

Tokay, A., P. G. Bashor, and K. R. Wolff (2005), Error characteristics of rainfall measurements by collocated Joss-Waldvogel Disdrometers, *J. Atmos. Oceanic Technol.*, *22*(5), 513–527, doi:10.1175/JTECH1734.1.

Tokay, A., W. A. Petersen, P. Gatlin, and M. Wingo (2013), Comparison of raindrop size distribution measurements by collocated disdrometers, *J. Atmos. Oceanic Technol.*, *30*(8), 1672–1690, doi:10.1175/JTECH-D-12–00163.1.

Ulbrich, C. W. (1983), Natural variations in the analytical form of the raindrop size distribution, *J. Clim. Appl. Meteorol.*, *22*(10), 1764–1775, doi:10.1175/1520-0450(1983)022<1764:NVITAF>2.0.CO;2.

Ulbrich, C. W. (1985), The effects of drop size distribution truncation on rainfall integral parameters and empirical relations, *J. Clim. Appl. Meteorol.*, *24*(6), 580–590, doi:10.1175/1520-0450(1985)024<0580:TEODSD>2.0.CO;2.

Ulbrich, C. W., and D. Atlas (1998), Rainfall microphysics and radar properties: Analysis methods for drop size spectra, *J. Appl. Meteorol.*, *37*(9), 912–923, doi:10.1175/1520-0450(1998)037<0912:RMARPA>2.0.CO;2.

Ulbrich, C. W., and D. Atlas (2007), Microphysics of raindrop size spectra: Tropical continental and maritime storms, *J. Appl. Meteorol. Climatol.*, *46*(11), 1777–1791, doi:10.1175/2007JAMC1649.1.

Uijlenhoet, R., and J. H. Pomeroy (2001), Raindrop size distributions and radar reflectivity-rain rate relationships for radar hydrology, *Hydrol. Earth Syst. Sci. Discuss.*, *5*(4), 615–628, doi:10.5194/hess-5–615-2001.

Uijlenhoet, R., and D. Sempere Torres (2006), Measurement and parameterization of rainfall microstructure, *J. Hydrol.*, *328*(1), 1–7, doi:10.1016/j.jhydrol.2005.11.038.

Uijlenhoet, R., M. Steiner, and J. A. Smith (2002), Influence of disdrometer deadtime correction on self-consistent analytical parameterizations for raindrop size distributions, in *Proceedings of ERAD*, vol. 1, pp. 104–112, Copernicus. [Available at http://copernicus.org/erad/online/erad-104.pdf.]

Uijlenhoet, R., M. Steiner, and J. A. Smith (2003), Variability of raindrop size distributions in a squall line and implications for radar rainfall estimation, *J. Hydrometeorol.*, *4*(1), 43–61, doi:10.1175/1525–7541(2003)004<0043:VORSDI>2.0.CO;2.

Vargo, E., R. Pasupathy, and L. M. Leemis (2010), Moment-ratio diagrams for univariate distributions, *J. Qual. Technol.*, *42*, 276–286.

Venables, W. N., and B. D. Ripley (2002), *Modern Applied Statistics With S*, 4th ed., Springer, New York, ISBN: 0–387-95457-0.

Villermaux, E., and B. Bossa (2009), Single-drop fragmentation determines size distribution of raindrops, *Nat. Phys.*, *5*, 697–702, doi:10.1038/nphys1340.

Vivekanandan, J., G. Zhang, and E. Brandes (2004), Polarimetric radar estimators based on a constrained Gamma drop size distribution model, *J. Appl. Meteorol.*, *43*(2), 217–230, doi:10.1175/1520-0450(2004)043<0217:PREBOA>2.0.CO;2.

Wagenmakers, E.-J., and S. Farrell (2004), AIC model selection using Akaike weights, *Psychonomic Bull. Rev.*, *11*(1), 192–196, doi:10.3758/BF03206482.

Wakazuki, Y. (2013), Modified relative humidity based on the Johnson's SB distribution function, *SOLA*, *9*, 111–114, doi:10.2151/sola.2013-025.

Waldvogel, A. (1974), The n0 jump of raindrop spectra, *J. Atmos. Sci.*, *31*(4), 1067–1078, doi:10.1175/1520-0469(1974)031<1067:TJORS>2.0.CO;2.

Williams, C. R., and K. S. Gage (2009), Raindrop size distribution variability estimated using ensemble statistics, *Ann. Geophys.*, *27*, 555–567, doi:10.5194/angeo-27–555-2009.

Willis, P. T. (1984), Functional fits to some observed drop size distributions and parameterization of rain, *J. Atmos. Sci.*, *41*, 1648–1661, doi:10.1175/1520-0469(1984)041<1648:FFTSOD>2.0.CO;2.

Withers, C. S., and S. Nadarajah (2011), Bias-reduced estimates for skewness, kurtosis, L-skewness and L-kurtosis, *J. Stat. Plann. Inference*, *141*(12), 3839–3861, doi:10.1016/j.jspi.2011.06.024.